IOP Publishing Physica Scripta
Phys. Scr. **T130** (2008) 014029 (6pp) doi:10.1088/0031-8949/2008/T130/014029

The effects of young embedded groups and clusters on forming solar systems

Fred C Adams

Physics Department, University of Michigan, Ann Arbor, MI 41809, USA

E-mail: fca@umich.edu

Received 11 March 2008
Accepted for publication 14 March 2008
Published 16 July 2008
Online at stacks.iop.org/PhysScr/T130/014029

Abstract
Most stars—and hence most solar systems—form within groups or clusters. This contribution discusses how these star forming environments affect the planetary systems forming within them. The discussion starts with the dynamical evolution of young stellar clusters with $N = 100$–1000 members. We use N-body simulations to explore how evolution depends on system size N and the initial conditions. Motivated by recent observations, this study compares subvirial and virial starting states. Multiple realizations of equivalent cases (100 simulations per case) are used to build up a robust statistical description of these systems, e.g. distributions of closest approaches and distributions of radial locations. These results provide a framework from which to assess the effects of clusters on planet formation. The distributions of radial positions are used in conjunction with far ultraviolet (FUV) luminosity distributions to determine the radiation exposure of circumstellar disks. Photoevaporation calculations then determine the efficacy of radiation in removing gas from the systems (resulting in loss of planet forming potential). The distributions of closest approaches are used in conjunction with scattering cross-sections (calculated from 100 000 numerical experiments) to determine the probability of solar system disruption. Our main result is that clusters in this size range can have a significant effect on forming planetary systems, and we have quantified the size of these effects. For example, in modest-sized clusters, FUV radiation typically leads to disk photoevaporation down to outer disk radii of 30–50 AU.

PACS numbers: 95.10.Fh, 96.12.Bc, 97.10.Bt, 97.10.Gz, 98.20.−d

1. Introduction

Although a working theory of star formation has been constructed over the past two decades (e.g. Shu *et al* 1987), most of the theoretical development applies specifically to the formation of isolated stars. In contrast, recent observational work has underscored the fact that most star formation takes place in embedded stellar groups and clusters (e.g. Lada and Lada 2003, Porras *et al* 2003), although an unambiguous specification of the the size distribution remains elusive. Given that most stars form in clusters of some membership size N, two overarching questions arise. The first considers the clusters as astrophysical objects: (i) how can molecular clouds produce aggregates of $N > 100$ stars with centrally concentrated surface density, with the most massive stars near the center, and with a stellar mass distribution that follows the initial mass function (IMF), all within $\sim$1 pc and within $\sim$1 Myr? The second vital question then becomes: (ii) if stars form in clusters, how does the cluster environment affect star formation and the accompanying process of planet formation? Although a complete understanding of star and planet formation requires detailed answers to both questions, this paper focuses on the second issue. Furthermore, although clusters come with a wide range of stellar membership N, this work focuses on clusters with intermediate sizes $N = 100$–1000. This choice is motivated by the current observational census of star forming clusters in the solar neighborhood, as shown in figure 1.

This paper is organized as follows. We begin, in section 2, by considering N-body simulations of the cluster environment. The results of these calculations are used to determine the interaction rates for close encounters between cluster members and the probability distribution for radial positions within the clusters. This latter quantity helps determine the radiation exposure experienced by star/disk systems. This issue is considered further in section 3, which

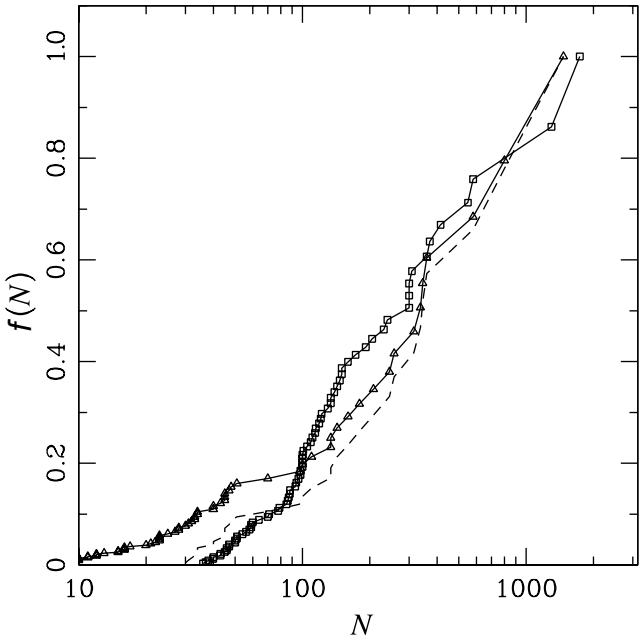

Figure 1. Cumulative distribution of group/cluster sizes as a function of system size N. The quantity $f(N)$ is the fraction of the total number of stars in the sample that live in groups/clusters of system size N or smaller. The curve marked by open squares corresponds to the 2 kpc sample, which is complete down to $N = 30$ (Lada and Lada 2003); the curve marked by open triangles is the 1 kpc sample, which is complete down to $N = 10$ (Porras *et al* 2003). The dashed curve shows the 1 kpc sample subjected to the same selection criteria as the 2 kpc sample.

culminates in the construction of the probability distribution for FUV radiation flux. With the radiation exposure quantified, we consider the effects of photoevaporation in section 4. In section 5, we present the results for the cross-sections for disruption of young solar systems by passing stars and binaries. We conclude, in section 6, with a summary of the effects of young embedded groups and clusters on the process of planet formation.

2. Results from N-body simulations

In this section, we present a brief overview of the N-body simulations (see Adams *et al* 2006 for greater detail). This work was done using N-body codes from the series written by S Aarseth (1999, 2001, 2003), although a number of modifications were required. This section presents the results from six classes of clusters, with stellar membership chosen to be $N = 100$, 300 and 1000, and with both virial and subvirial starting conditions. The latter class of starting conditions is motivated by recent observations of star forming regions (e.g. Walsh *et al* 2004).

2.1. Initial conditions

To set the cluster radius R_{c^*} for a given size N, we use the observed correlation, which can be fit by the relation of the form

$$R_{c^*}(N) = R_{300}\sqrt{(N/300)}, \qquad (1)$$

where $R_{300} \approx 1$–2 pc. This relation corresponds to a nearly constant surface density of stars $N/R^2 \approx$ constant (e.g. Adams *et al* 2006, Carpenter 2000, Lada and Lada 2003).

Observations of young embedded clusters indicate that the gas density profiles may have (roughly) the form $\rho \sim r^{-1}$ (e.g. Jijina *et al* 1999, Larson 1985) on the radial scale of the cluster ($\sim$1 pc). For these simulations we need to include the gravitational potential of the gaseous component and eventually let it disappear with time. In order to smoothly extend the initial gas potential out to large radii, we adopt a Hernquist profile so that the initial gas distribution is characterized by the potential, density and mass profiles of the forms

$$\Psi = \frac{2\pi G\rho_0 r_s^2}{1+\xi}, \qquad \rho = \frac{\rho_0}{\xi(1+\xi)^3} \qquad \text{and} \qquad M = \frac{M_\infty \xi^2}{(1+\xi)^2}, \qquad (2)$$

where $\xi \equiv r/r_s$ and r_s is a scale length (Hernquist 1990). Notice that $M_\infty = 2\pi r_s^3 \rho_0$. In practice, we identify the scale r_s with the cluster size (equation (1)), so that $r_s = R_{c^*}$. The density profile within the cluster itself thus has the form $\rho \sim r^{-1}$; the steeper density dependence $\rho \sim r^{-4}$ occurs only at large radii (effectively outside the cluster) and allows the potential to smoothly join onto a force-free background. The gas is allowed to stay in the cluster system for 5 Myr, and is then considered to be dispersed. Star formation (the introduction of stars into the cluster) takes place over a shorter time interval of 1 Myr. The cluster simulations are then run for a total integration time of 10 Myr. All of these timescales have some uncertainties, but are roughly consistent with current observational constraints (Allen *et al* 2006).

2.2. Output distributions

As one way to characterize the evolution of these systems, we produce mass profiles $M(r)$ averaged over the 10 Myr time interval of interest. Specifically, the radial position of every star is recorded at intervals of 0.25 Myr throughout each simulation. The resulting data set is used to create a mass profile $M(r)/M_{T^*}$ at each time, where M_{T^*} is the total mass in stars that remain bound. The profiles are then averaged over all time steps and averaged over the 100 equivalent realizations of the system to produce the radial mass profile associated with each type of group/cluster. The integrated mass distribution $M(r)$ can be fit with a simple function of the form

$$\frac{M(\xi)}{M_{T^*}} = \left(\frac{\xi^a}{1+\xi^a}\right)^p, \qquad (3)$$

where $\xi = r/r_0$, and where the scale length r_0 and the index p are free parameters that are fit to the output of the simulations.

The cluster environment facilitates close stellar encounters which can disrupt solar systems. Within the ensemble of N-body simulations described above, we can find the distributions of close encounters. These distributions, in conjunction with the cross-sections for disruptions of planetary systems, binary-disk systems and binary-star interactions can then be used to estimate the probability of interactions as a function of system size N (and other initial conditions). Specifically, the close encounters for each star are tracked throughout each cluster simulation; the resulting data is labeled with both stellar mass and cluster age. The total distribution of closest approaches for each simulation is calculated, and these distributions are then averaged over the

100 equivalent realizations of the system. The result is an integrated distribution of closest approaches for each type of cluster. The results are presented in terms of an interaction rate, i.e. the number of close encounters with $r \leqslant b$ that the 'typical star' experiences per million years (1 Myr is a convenient unit of time and is approximately the cluster crossing time). This interaction rate is a function of closest approach distance b and can be fit with an expression of the form

$$\Gamma = \Gamma_0 \left(\frac{b}{1000\,\mathrm{AU}} \right)^{\gamma} . \qquad (4)$$

The rate Γ is thus the number of close encounters with $r \leqslant b$ per star per million years. Note that b is the distance of closest approach—the minimum distance during the flyby—and is thus generally smaller than the impact parameter of the encounter. For an interaction rate of the form of equation (4), and for a 10 Myr time span, the 'typical' star will experience (on average) one encounter with the characteristic impact parameter b_C given by

$$b_C \equiv 1000\,\mathrm{AU}\,(10\Gamma_0)^{-1/\gamma} . \qquad (5)$$

For the six classes of clusters considered here, the characteristic impact parameter lies in the range $b_C =$ 700–4000 AU. Note that the results quoted here were obtained using the entire population of stars, i.e. stars of all masses. However, interactions depend on stellar masses and clusters eventually become mass segregated. As a result, the interaction rate for stars of a particular mass have the general form of equation (4), but the values of the parameters (Γ_0, γ) will vary with mass.

3. Distributions of radiation fields

In this section, we estimate the radiation fields provided by young embedded clusters. Both FUV and extreme ultra-violet (EUV) radiation can drive evaporation from circumstellar disks and cause the loss of planet forming potential (Armitage 2000, Johnstone *et al* 1998, Shu *et al* 1993), but this section focuses on FUV (see Adams *et al* 2004). The resulting distribution of FUV flux is shown in figure 2. Calculation of the FUV radiation is complicated by many factors: first and foremost, the result is a distribution, i.e. the probability that a given solar system will experience a given radiation flux as a function of flux. The determination of this distribution requires specification of three input distributions: (i) the distribution of cluster membership N, (ii) the distribution of FUV luminosity for clusters with a given N, and (iii) the distribution of radial positions within a cluster, including the star/disk systems being evaporated and the massive stars that dominate the production of UV radiation. To obtain the benchmark distribution shown in figure 2, we used the observed compilation of nearby clusters (Lada and Lada 2003, figure 1) to specify the distribution of cluster membership N, and random sampling of the stellar IMF to specify the distribution of FUV luminosity for a given cluster membership N. The radial positions of star/disk systems were sampled from a stellar density profile of the form $\rho^* \sim 1/r$, roughly consistent with our N-body simulations (see section 2). The massive stars were assumed to reside at the cluster center, consistent with observations

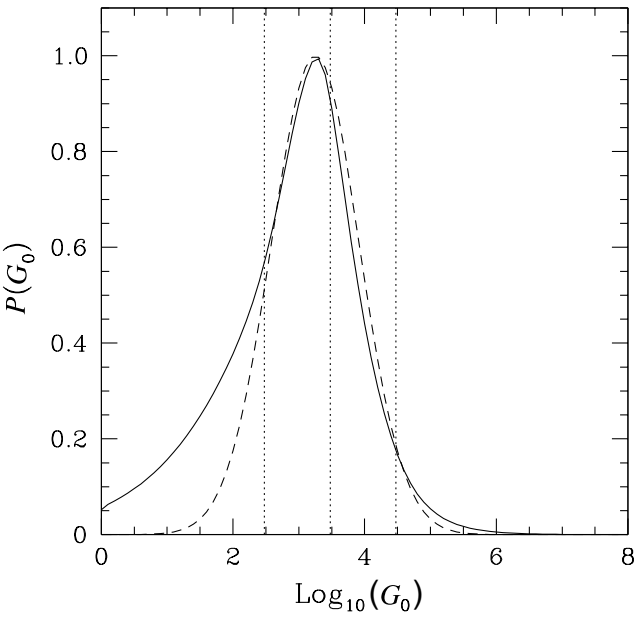

Figure 2. Probability distribution for FUV flux experienced by the ensemble of cluster stars as a function of the FUV flux, expressed here in units of G_0 (where $G_0 = 1$ corresponds to a flux of 1.6×10^{-3} erg s^{-1} cm^{-2}, which is close to the value of the interstellar radiation field). The ensemble distribution was calculated assuming that the number of stars living in groups/clusters of size N follows the distribution of figure 1, the radial size R_{c^*} of clusters follows the distribution of equation (1), the distribution of FUV luminosity results from sampling the IMF, and the density distribution within the cluster has the simple form $\rho_* \propto r^{-1}$ for $0 \leqslant r \leqslant R_{c^*}$.

(Testi *et al* 1999). Since high mass stars evolve quickly to the main-sequence and provide most of the relevant radiation, this work used standard stellar models to specify the radiative output (Maeder and Meynet 1987, Schaller *et al* 1992). Attenuation was not included so that target solar systems receive the full UV flux of radiation.

The resulting distribution of FUV flux is shown in figure 2. The solid curve shows the composite distribution, constructed using the distributions of cluster sizes, IMF sampling and stellar positions, as described above. The dashed curve shows a gaussian distribution with the same peak location (at $\log_{10} G_0 = 3.25$) and the FWHM (1.575). The calculated distribution has a significant tail at low flux values. The vertical lines at $G_0 = 300, 3000$ and 30 000 are benchmark values for which the effects of photoevaporation on circumstellar disks has been calculated in detail (see Adams *et al* 2004 and section 4).

4. Photoevaporation due to FUV radiation

When stars form within moderate-sized groups and clusters, (with $N_\star \approx$ 100–1000 members), their circumstellar disks are exposed to relatively little EUV ($h\nu > 13.6$ eV) radiation but a great deal of FUV (6 eV $< h\nu <$ 13.6 eV) radiation ($\sim 10^3$ times the local interstellar FUV field) from the most massive stars in the group. This section calculates the mass loss rates and evaporation timescales for circumstellar disks exposed to external FUV radiation (Adams *et al* 2004). Previous work (e.g. Störzer and Hollenbach 1999) treated large disks and/or

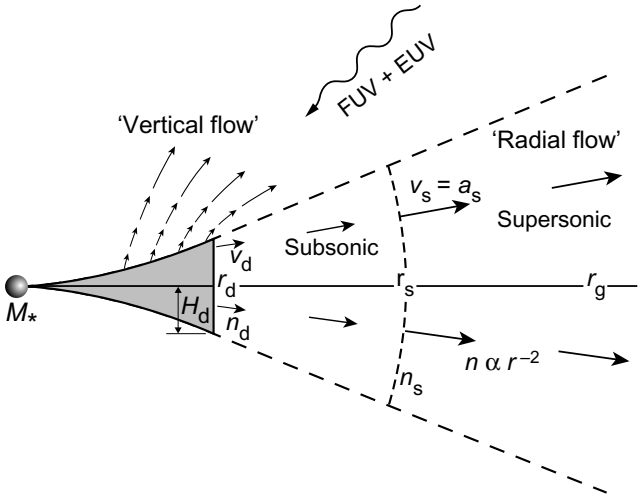

Figure 3. Schematic diagram of a disk with radius r_d around a star with mass M_*, illuminated by the FUV (and perhaps EUV) radiation from nearby stars. The disk is inclined so that the top and edge are exposed. The disk scale height is H_d at the outer radius r_d. In the subcritical regime, where $r_d < r_g$, the bulk of the photoevaporation flow (the radial flow) originates from the disk edge, which marks the inner boundary.

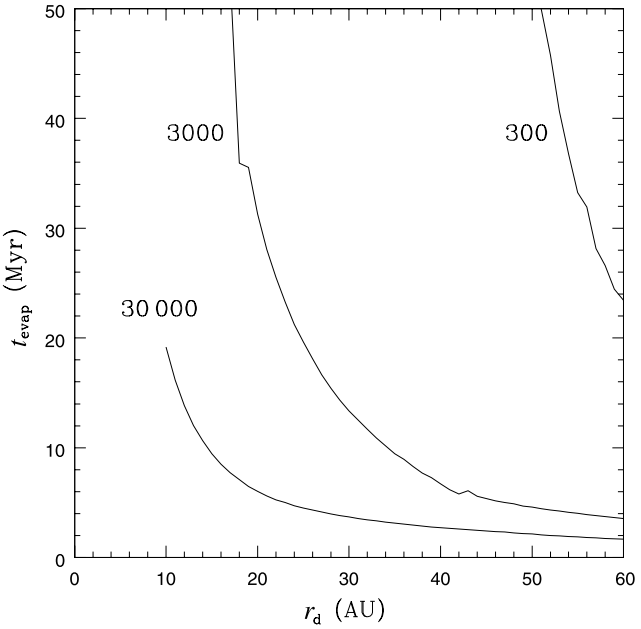

Figure 4. Photoevaporation timescales for circumstellar disks exposed to varying external radiation fields, $G_0 = 300$, 3000 and 30 000 (as labeled). These models assume that the disk orbit around central stars with mass $M_* = 1.0\ M_\odot$.

intense radiation fields for which the disk radius r_d exceeds the critical radius r_g where the sound speed in the FUV heated surface layer exceeds the escape speed. Most previous work has assumed that photoevaporation occurs for $r_d > r_g$ and is negligible for $r_d < r_g$. Since $r_g \gtrsim 100$ AU for FUV heating, this would imply little mass loss from the planet-forming regions of a disk. As shown by Adams *et al* (2004), however, for systems in which photoevaporation is suppressed because $r_d < r_g$, significant mass loss still takes place as long as $r_d/r_g \lesssim 0.1$–0.2. The reason for this is straightforward: some of the gas extends beyond the disk edge (or above the disk surface) to larger distances where the temperature is higher, the escape speed is lower, and an outflow develops. The resulting evaporation rate is a sensitive function of the central stellar mass and disk radius, which determine the escape speed; the evaporation rate also is sensitive to the intensity of the external FUV flux, which determines the temperature structure of the surfaces layers and outflowing gas.

A schematic diagram of this process in shown in figure 3. The flow begins subsonically at outer disk edge r_d, and then accelerates to the sound speed at r_s (the sonic point), which lies inside the critical escape radius r_g. Beyond the sonic point, the flow attains a terminal speed of order the sound speed and the density falls roughly as $n \propto r^{-2}$. Although some material is lost off the top and bottom faces of the disk (in a vertical flow), its contribution to the mass loss rate is secondary to that from the edges. Nonetheless, the polar regions are not evacuated, the star is fully enveloped by circumstellar material, and the incoming FUV radiation will be attenuated in all directions. With the geometry specified, the evaporation rates $\dot{M}$ are calculated according to the formulation of Adams *et al* (2004). To convert the mass loss rate into an evaporation timescale, we assume that disks have masses $M_d = 0.05 M_* \ (r_d/30\ \mathrm{AU})^{1/2}$, i.e. about twice the minimum mass solar nebula for a solar type star. The evaporation timescales are thus proportional to the disk mass, $t_{evap} \propto M_d$. The resulting timescales for disk evaporated are shown in figure 4. Notice that a radiation field of $G_0 = 300$ has little effect on disks surrounding solar type stars. On the other hand, an FUV radiation field with $G_0 = 3000$ will evaporate the outer parts of the disk down to ∼36 AU in 10 Myr. Notice that the disk lifetime will be shorter than this 'evaporation time' because the inner parts of the disk are drained onto the star through viscous accretion. Notice also that the radiative flux $G_0 = 3000$ is near the peak of the expected distribution of FUV fluxes, as shown in figure 2. For even larger fields, $G_0 = 30\,000$, the FUV radiation is highly destructive and truncates disks down to ∼12 AU over 10 Myr. Although the region of the disk where Jupiter now resides ($\varpi \sim 5$ AU) is generally safe from photoevaporation, disks that live in intense radiation environments will experience substantial mass loss.

The above discussion applies to solar type stars. Disks around red dwarfs, low mass stars with $M^* \lesssim 0.5\ M_\odot$, are evaporated more readily. They will shrink to disk radii $r_d \lesssim 15$ AU on timescales $t \lesssim 10$ Myr when exposed to moderate FUV fields with $G_0 = 3000$ (where $G_0 = 1.7$ for the local interstellar FUV field). The disks around solar type stars are more durable. For intense FUV radiation fields with $G_0 = 30\,000$, however, even these disks shrink to $r_d \lesssim 15$ AU on timescales $t \sim 10$ Myr. Such fields exist within about 0.7 pc of the center of a cluster with $N_\star \approx 4000$ stars. If our solar system formed in the presence of such strong FUV radiation fields, this mechanism could explain why Neptune and Uranus in our solar system are gas poor, whereas Jupiter and Saturn are relatively gas rich. This mechanism for photoevaporation can also limit the production of Kuiper belt objects and can suppress giant planet formation in sufficiently large clusters, such as the Hyades, especially for disks associated with low mass stars. Finally, we note that radiation exposure depends on the orbit of the star/disk system through its

cluster; orbit-averaged fluxes can be calculated from the orbit solutions of Adams and Bloch (2005).

5. Scattering cross-sections and implications

The N-body simulations of section 2 produce estimates for the interaction rates of cluster members. Given this interaction rate, one can determine what effects such interactions can have on circumstellar disks and newly formed solar systems. Such effects must be given in terms of probability distributions. To complete the specification of the problem, however, we need to know the cross-sections for interactions to disrupt the solar systems.

In this brief summary, we consider two types of interactions. In the first, stars with circumstellar disks encounter other stellar members. Previous work shows that such encounters will truncate the disks (through gas removal) down to radii that are approximately one third of the distance of closest approach (Kobayashi and Ida 2001). Since the 'typical' distances of closest approach are found to lie in the range $b_C = 710$–3650 AU, we predict that disks will be truncated to outer radii in the range $r_D = 240$–1200 AU. Notice that the effects of photoevaporation, as outlined in the previous section, are generally more severe.

The other way for interactions to disrupt solar systems is through interactions with planetary systems that are already formed. To study this process we calculate the cross-sections through a Monte Carlo procedure developed previously (Adams and Laughlin 2001, Laughlin and Adams 2000). The results are shown in figure 5, which shows the cross-sections for increasing the eccentricity of planetary orbits, given here as a function of the eccentricity increase. The four panels in the figure correspond to four choices of the stellar mass. The four lines in each panel correspond to the results for four planets, which are taken to have the masses and semi-major axes of the giant planets in our Solar System. The end of the curves at $e = 1$ corresponds to loss of the planet, either through ejection or capture. These ejection cross-sections can be summarized through a simple fitting function of the form

$$\langle \sigma \rangle_{\rm eject} \approx \mathcal{C}_0 \, (a_{\rm p}/{\rm AU}) (M_*/M_\odot)^{-1/2}, \qquad (6)$$

where the constant $\mathcal{C}_0 \approx 1350 \pm 150$ AU^2, where this uncertainty range results from the variation across the different planets and varying stellar masses. The uncertainties arising from Monte Carlo scattering errors are an order of magnitude smaller. From this set of cross-sections, for example, we can estimate the number of 'rogue' planets expected in a typical cluster due to stellar encounters with newly formed solar systems. The ejection rate of Jupiter analogs is about 0.15 ejections per cluster per million year. Thus, over a typical 10 Myr life-span of a cluster, one expects only one or two Jupiters to be ejected. This number is not only small, but it is much smaller than the number of planets expected to be ejected from planet–planet scattering within solar systems.

On a related note, the recent discovery of the trans-neptunian object Sedna (Brown *et al* 2004) raises interesting questions about the possible effects of scattering interactions on our own solar system. Sedna has a highly eccentric orbit with perihelion $p = a(1 - e) = 70$ AU and is thus rather unusual among solar system bodies. Numerical simulations indicate that a passing star could have scattered Sedna from the Kuiper belt into its observed eccentric orbit (Brasser *et al* 2006, Kenyon and Bromley 2004, Morbidelli and Levison 2004), roughly similar to the scattering interactions considered here.

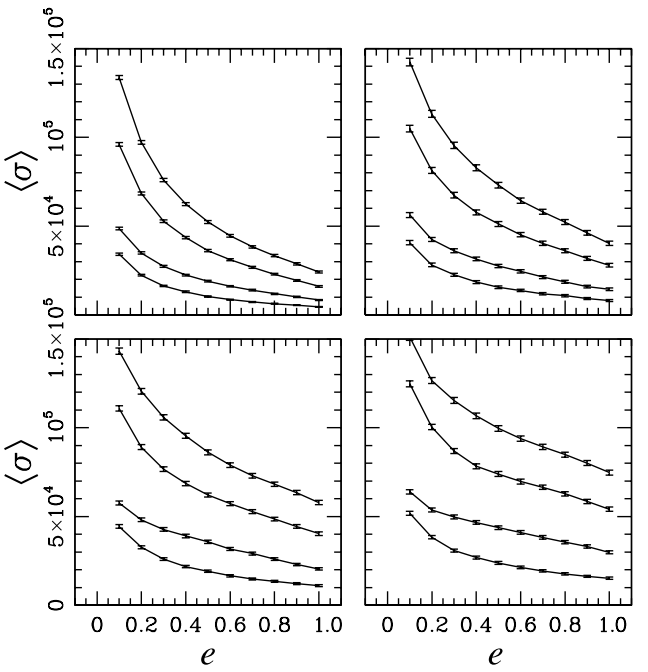

Figure 5. Scattering cross-sections for solar systems to increase the eccentricity e of planetary orbits, plotted here as a function of eccentricity. All cross-sections are given in units of (AU) ^{2}. The four panels shown here correspond to the four largest stellar mass values of our computational survey, i.e. $M_* = 2.0\, M_\odot$ (upper left) $1.0\, M_\odot$ (upper right), $0.5\, M_\odot$ (lower left) and $0.25\, M_\odot$ (lower right). In each panel, the four curves shown correspond to four giant planets orbiting the central star, where the planets have the same masses and starting semimajor axes as the giant planets in our solar system. The top curve in each panel corresponds to an analog of Neptune and the bottom curve corresponds to an analog of Jupiter. The cross-section for increasing the eccentricity beyond unity (right end points of the curves) corresponds to ejection of the planet. The error bars correspond to the uncertainties incurred due to the (incomplete) Monte Carlo sampling of the parameter space.

6. Conclusions

This paper presents an assessment of the effects of clusters on planet formation. The cluster environment affects circumstellar disks (the birth sites for planets) in two ways: close encounters between star/disk systems and other cluster members results in disk truncation. Given the distributions of close encounters calculated herein, we estimate that typical disks are truncated down to outer radii of a few 100 AU through this process. The clusters also affect disks through their radiation fields. In modest-sized clusters, such as those found in the solar neighborhood, FUV radiation dominates this process and leads to disk evaporation down to outer disk radii of 30–50 AU. This outer truncation, in conjunction with disk accretion through viscous spreading, can account for the observed (relatively short) disk lifetimes. Finally,

we stress that the results of most of these processes must be considered as distributions: the amount of radiative flux that solar systems are exposed to will be a distribution (e.g. figure 2); the probability of a close encounter within a given closest approach will also be a distribution (e.g. equation (4)). This complication must be taken into account in any assessment of the effects of cluster environments on star and planet formation.

Acknowledgments

I would like to thank all of my collaborators involved in this research program, including Lori Allen, Tony Bloch, Marco Fatuzzo, Dave Hollenbach, Greg Laughlin, Tom Megeath, Phil Myers and Eva Proszkow. This work was supported at the University of Michigan through the Michigan Center for Theoretical Physics, and by NASA through the NASA Theory Program and the Spitzer Space Telescope Theory Program.

References

Aarseth S J 1999 *Publ. Astron. Soc. Pacific* **111** 1333
Aarseth S J 2001 *New Astron.* **6** 277
Aarseth S J 2003 *Gravitational N-Body Simulations* (Cambridge: Cambridge University Press)
Adams F C and Bloch A M 2005 *Astrophys. J.* **629** 204
Adams F C, Hollenbach D, Laughlin G and Gorti U 2004 *Astrophys. J.* **611** 360
Adams F C, Proszkow E M, Fatuzzo M and Myers P C 2006 *Astrophys. J.* **641** 504
Adams F C and Laughlen G 2001 *Icarus* **150** 151
Allen L *et al* 2006 *Protostars and Planets V* (Tucson: University Arizona Press) p 361
Armitage P J 2000 *Astron. Astrophys.* **362** 968
Brasser R, Duncan M J and Levison H F 2006 *Icarus* 58–82
Brown M E, Trujillo C and Rabinowitz D 2004 *Astrophys. J.* **617** 645
Carpenter J M 2000 *Astron. J.* **120** 3139
Hernquist L 1990 *Astrophys. J.* **356** 359
Jijina J, Myers P C and Adams F C 1999 *Astrophys. J. Suppl.* **125** 161
Johnstone D, Hollenbach D J and Bally J 1998 *Astrophys. J.* **499** 758
Kenyon S J and Bromley B C 2004 *Nature* **432** 598
Lada C J and Lada E A 2003 *Annu. Rev. Astron. Astrophys.* **41** 57
Larson R B 1985 *Mon. Not. R. Astron. Soc.* **214** 379
Laughlin G and Adams F C 2000 *Icarus* **145** 614
Maeder A and Meynet G 1987 *Astron. Astronphys.* **182** 243
Marcy G W and Butler R P 1996 *Astrophys. J.* **464** L147
Morbidelli A and Levison H F 2004 *Astron. J.* **128** 2564
Porras A *et al* 2003 *Astron. J.* **126** 1916
Schaller G, Schaerer D, Meynet G and Maeder A 1992 *Astron. Astrophys. Suppl.* **96** 269
Shu F H, Adams F C and Lizano S 1987 *Annu. Rev. Astron. Astrophys.* **25** 23
Shu F H, Johnstone D and Hollenbach D J 1993 *Icarus* **106** 92
Störzer H and Hollenbach D 1999 *Astrophys. J.* **515** 688
Testi L, Palla F and Natta A 1999 *Astron. Astrophys.* **342** 515
Walsh A J, Myers P C and Burton M G 2004 *Astrophys. J.* **614** 194